Phonon thermal conductivity of monolayer MoS_2: A comparison with single layer graphene

Cite as: Appl. Phys. Lett. **105**, 103902 (2014); https://doi.org/10.1063/1.4895344
Submitted: 21 June 2014 . Accepted: 22 August 2014 . Published Online: 08 September 2014

Xiaolin Wei, Yongchun Wang, Yulu Shen, Guofeng Xie, Huaping Xiao, Jianxin Zhong, and Gang Zhang

Phonon thermal conductivity of monolayer MoS_2: A comparison with single layer graphene

Xiaolin Wei,[1] Yongchun Wang,[1] Yulu Shen,[1] Guofeng Xie,[1,a)] Huaping Xiao,[1] Jianxin Zhong,[1] and Gang Zhang[2,a)]
[1]*Hunan Key Laboratory of Micro-Nano Energy Materials and Devices, Faculty of Materials, Optoelectronics and Physics, Xiangtan University, Hunan 411105, People's Republic of China*
[2]*Institute of High Performance Computing, Singapore 138632, Singapore*

(Received 21 June 2014; accepted 22 August 2014; published online 8 September 2014)

We investigate the size and edge roughness dependence on thermal conductivity of monolayer MoS_2 ($MLMoS_2$) by phonon Boltzmann transport equation combined with relaxation time approximation. The relative contribution of spectral phonons to thermal conductivity is explored, and we compared the characteristics of phonon transport with those in single layer graphene (SLG), which is a representative two-dimensional material. Quite different from SLG, because of the ultra-short intrinsic phonon mean free path, the thermal conductivity of $MLMoS_2$ ribbons is size and roughness insensitive. The LA phonons have the major contribution to thermal conductivity of $MLMoS_2$, and the ZA phonons in $MLMoS_2$ have high relative contribution to thermal conductivity. The relative contribution to thermal conductivity from both high frequency and low frequency phonons in $MLMoS_2$ is lower than that in SLG. The underlying mechanism of these distinct characteristics results from the different phonon dispersions and anharmonic characteristic between $MLMoS_2$ and SLG. © *2014 AIP Publishing LLC*. [http://dx.doi.org/10.1063/1.4895344]

Very recently, the thermal conductivity of monolayer MoS_2 ($MLMoS_2$), one of the most stable layered transition metal dichalcogenides (TMD), has attracted numerous interest.[1–7] Unlike graphene, $MLMoS_2$ is a semiconductor with a large bandgap, and hence, $MLMoS_2$ is regarded as a promising candidate for field effect transistor and optoelectronics device applications.[8,9] In electronic and energy device applications, highly efficient heat dissipation is critical for the device reliability and performance. On the other side, the large Seebeck coefficient[10] suggests potential applications of 2D MoS_2 as thermal energy harvesting and thermoelectric cooling. In thermoelectric application, low thermal conductivity is preferred. Although high power factor is also observed in graphene, the ultra-high thermal conductivity of graphene[11] offsets its advantages and limits application of graphene as efficient 2D thermoelectric materials. In contrast to the superior thermal conductivity of graphene,[11–14] the thermal conductivity of $MLMoS_2$ is low, which has been presented by theoretical analysis[1–4] and experimental measurements.[7]

While a number of studies have been performed, the knowledge of thermal conductivity of MoS_2 is still not enough and largely obscure. For instance, systematic investigations on various effects on thermal conductivity of graphene have been done, including impacts of isotopic doping, folding, grain boundary, vacancy, defects, surface functionalization, etc.[14] In monolayer 2D sheet, there are three acoustic phonon polarization branches, which are transverse-acoustic (TA), longitudinal-acoustic (LA), and out-of-plane acoustic (ZA) phonons. The frequency dependent contribution of different acoustic phonon modes to thermal conductivity of graphene has been widely addressed.[12–14] The phonon mean free path (MFP) and the relative contribution of spectral phonons to thermal conductivity are crucial towards understanding and engineering the thermal conductivity of nanostructures,[15–17] however, these knowledge of $MLMoS_2$ are scarce so far. Furthermore, the size and roughness dependence of thermal conductivity for $MLMoS_2$ and the underlying mechanism have not been well studied.

In this letter, by combining phonon Boltzmann transport equation (BTE) with relaxation time approximation and adopting first-principles calculations predicted phonon dispersions and Grüneisen parameters,[4] we investigate the effects of size, roughness, and temperature on the thermal conductivity of spectral phonons, as well as the intrinsic phonon MFP for $MLMoS_2$. Unlike the strong size and edge roughness dependent thermal conductivity of single layer graphene (SLG), the thermal conductivity of $MLMoS_2$ ribbon is size and roughness insensitive, because of the ultra-short intrinsic phonon MFP (14.6 nm at room temperature). Furthermore, we analyze comprehensively the relative contribution of spectral phonons to heat conduction. It is found that at room temperature, the relative contribution of ZA phonons to the thermal conductivity is about 33%, and the relative contribution of TA phonons to thermal conductivity is only 7.5%, which is remarkably lower than that for SLG. It is also revealed by the normalized accumulative distribution of thermal conductivity that the relative contribution to thermal conductivity of both low frequency acoustic phonons (near the center of the first Brillouin zone) and high frequency acoustic phonons (near the edge of the first Brillouin zone) in $MLMoS_2$ is much lower than that in SLG. Our findings are helpful for understanding and engineering the thermal conductivity of $MLMoS_2$ sheet and nanoribbons.

According to linearized phonon BTE within relaxation time approximation, the thermal conductivity in branch λ of $MLMoS_2$ in the y direction (the longitudinal direction of ribbon) is derived as

[a)]Authors to whom correspondence should be addressed. Electronic addresses: gfxie@xtu.edu.cn and zhangg@ihpc.a-star.edu.sg

$$\kappa_\lambda = \frac{S}{(2\pi)^2}\int c_{ph} v_{\lambda,y}^2 \tau_\lambda d\vec{q} = \frac{S}{(2\pi)^2}\int_0^{q_{\max}}\int_0^{2\pi} \frac{k_B}{S\delta}\frac{\left[\hbar\omega_\lambda(q)/k_BT\right]^2 e^{\hbar\omega_\lambda(q)/k_BT}}{\left[e^{\hbar\omega_\lambda(q)/k_BT}-1\right]^2} \times v_\lambda^2(q)\cos^2\theta\tau_\lambda(q,\theta)qd\theta dq, \quad (1)$$

where $\lambda = LA$, TA, and ZA and only acoustic branches are considered. S is the area of the sample, c_{ph} is the volumetric specific heat of each mode, $v_{\lambda,y}$ is the y component of the group-velocity vector in branch λ, τ_λ is the averaged phonon relaxation time between successive scattering events of branch λ, $\vec{q}$ is the wave vector, $\delta = 0.441$ nm is the effective layer thickness,[18] θ (ranging from 0 to 2π) is the angle between the wave vector and y axis, and $q_{\max}$ is the cut-off wave vector.

The first-principle calculations show that the linear dispersion for in-plane acoustic branches and quadratic dispersion for out-of-plane acoustic branch, which are adopted in our previous work of graphene,[19,20] are not valid for $MLMoS_2$. Therefore, the $\omega_\lambda(q)$ and group velocity $v_\lambda(q)$ are adopted from the fitted phonon dispersion curves based on the previous first-principle calculations.[4]

The Matthiessen's rule is applied to combine the effects of phonon-phonon Umklapp scattering (τ_U) and phonon-boundary scattering (τ_B), therefore

$$\tau_\lambda^{-1}(q,\theta) = \tau_{U,\lambda}^{-1}(q) + \tau_{B,\lambda}^{-1}(q,\theta). \quad (2)$$

The relaxation time of Umklapp phonon-phonon scattering was derived using an expression from Refs. 21 and 22 but introducing separate lifetimes for LA, TA, and ZA phonons

$$\tau_{U,\lambda}(q) = \frac{M v_\lambda^2(q)\omega_{D,\lambda}}{\gamma_\lambda^2(q)k_BT\omega_\lambda^2(q)}, \quad (3)$$

where M is the mass of a MoS_2 unit cell and $\gamma_\lambda(q)$ is the Grüneisen parameter, which controls the strength of the phonon-phonon scattering process for each branch. The first-principle calculations demonstrate that the Grüneisen parameters for all acoustic branches of $MLMoS_2$ have very strong dependence on wave vector.[4]

In order to explore the size and roughness dependence of thermal conductivity for $MLMoS_2$, we introduce the direction-dependent averaged relaxation time of phonon-boundary scattering, which was derived in details in our previous work[19,23]

$$\tau_{B,\lambda}(q,\theta) = \begin{cases} l_l(\theta)/v_\lambda(q) & \text{if } l_l < l_e \text{ and } \xi > P \\ l_e(\theta)/v_\lambda(q) & \text{otherwise,} \end{cases} \quad (4)$$

where l_e is the averaged distance traveled ballistically by a phonon before hitting the end boundary of the ribbon and l_l is the averaged distance traveled ballistically by a phonon before hitting the lateral boundary of the ribbon. ξ is a random number ranging from 0 to 1. If $\xi \le P$, the phonon boundary scattering is specular, otherwise the scattering is diffuse. The specularity parameter P is given as[24,25]

$$P = \exp(-4q^2\delta^2), \quad (5)$$

where δ is the root-mean-square (rms) value of the edge roughness fluctuations of the ribbon. Based on the assumption that the spatial distribution of phonons in the rectangular ribbon is uniform, l_e and l_l are given as follows:

$$l_e(\theta) = \frac{1}{L|\cos\theta|}\int_0^L ydy = \frac{L}{2|\cos\theta|}, \quad (6)$$

$$l_l(\theta) = \frac{1}{W|\sin\theta|}\int_0^W xdx = \frac{W}{2|\sin\theta|}, \quad (7)$$

where L is the length of the ribbon and W is the width of the ribbon.

The integral calculation of the thermal conductivity for $MLMoS_2$ according to Eq. (1) cannot be carried out analytically, but it can be performed by Monte Carlo sampling method, which is given as

$$\kappa_\lambda = \frac{k_B q_{\max}}{2\pi\delta}\cdot\frac{1}{N}\sum_{i=1}^{N} g_\lambda(q_i,\theta_i,\xi_i), \quad (8)$$

where N is the sampling number, and must be sufficiently large (for example, $N = 10^6$) in order to improve the accuracy and reduce the variance. $g_\lambda(q,\theta,\xi)$ is the integral function, which is expressed as

$$g_\lambda(q,\theta,\xi) = \frac{\left[\hbar\omega_\lambda(q)/k_BT\right]^2 e^{\hbar\omega_\lambda(q)/k_BT}}{\left[e^{\hbar\omega_\lambda(q)/k_BT}-1\right]^2} v_\lambda^2(q)\cos^2\theta\tau_\lambda(q,\theta)q. \quad (9)$$

q, θ, and ξ are uniform distribution in the range of $[0, q_{\max}]$, $[0, 2\pi]$, and [0,1], respectively.

Fig. 1(a) shows the room temperature thermal conductivity of LA, TA, and ZA phonons in $MLMoS_2$ with length up to 20 μm. The thermal conductivity contributions from TA and ZA phonons are independent on length, while that from LA phonons increases slightly with length, and thermal conductivity from these three modes converges with the length of ribbon when length is larger than 5 μm. The total thermal conductivity of $MLMoS_2$ at room temperature is about 26.2 W/mK, which is consistent with the measurements from the temperature-dependent Raman spectroscopy,[7] as well as the calculations from the nonequilibrium Green's function.[4] Figs. 1(b) and 1(c) give the width insensitive and edge roughness insensitive thermal conductivity of spectral phonons in $MLMoS_2$. The thermal conductivity of SLG sheet is strong size and edge roughness dependent, which has been demonstrated by theoretical[26–29] and experimental investigation.[30] The distinctions origin from the greatly different intrinsic phonon MFP between $MLMoS_2$ and SLG.

According to phonon-phonon Umklapp scattering, the intrinsic free path of phonons with wave vector q in branch λ is given as $\Lambda_\lambda(q) = v_\lambda(q)\cdot\tau_{U,\lambda}(q)$, and the intrinsic phonon MFP in branch λ is derived as

$$\bar{\Lambda}_\lambda = \frac{\int_0^{q_{\max}} \Lambda_\lambda(q)\cdot\frac{S}{(2\pi)^2}\cdot\frac{1}{e^{\hbar\omega_\lambda(q)/kT}-1}\cdot 2\pi q\cdot dq}{\int_0^{q_{\max}}\frac{S}{(2\pi)^2}\cdot\frac{1}{e^{\hbar\omega_\lambda(q)/kT}-1}\cdot 2\pi q\cdot dq}, \quad (10)$$

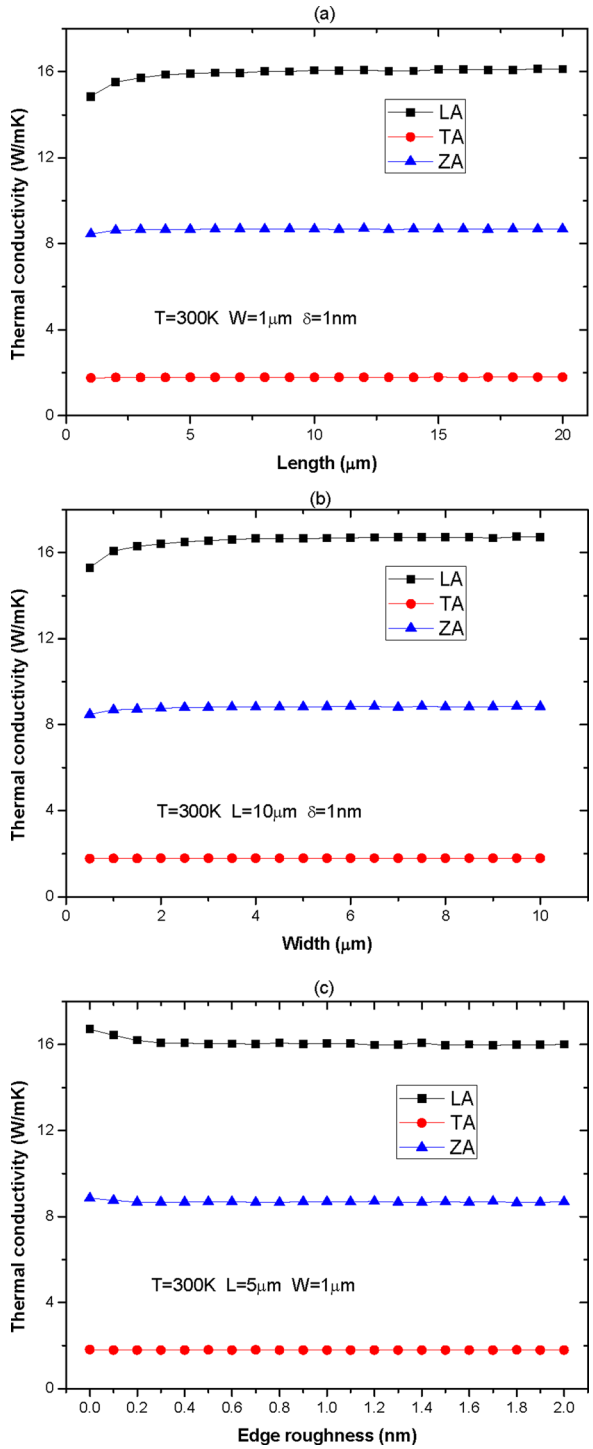

FIG. 1. The length (a), width (b), and edge roughness (c) dependence on thermal conductivity of $MLMoS_2$.

where $\frac{S}{(2\pi)^2}$ is the density of state in reciprocal space and $\frac{1}{e^{\hbar\omega_\lambda(q)/kT}-1}$ is the Bose-Einstein distribution function. Based on Eqs. (10) and (3), the intrinsic phonon MFP of acoustic branches as function of temperature are illustrated in Fig. 2. At room temperature, the intrinsic phonon MFP of LA, TA, and ZA branches are 49.1 nm, 6.4 nm, and 8.7 nm, respectively. All of them are far less than the size of ribbon (μm) considered in Fig. 1. Fig. 3 presents the rate of Umklapp scattering and phonon-boundary scattering of LA, TA, and ZA spectral phonons. The phonon-phonon Umklapp

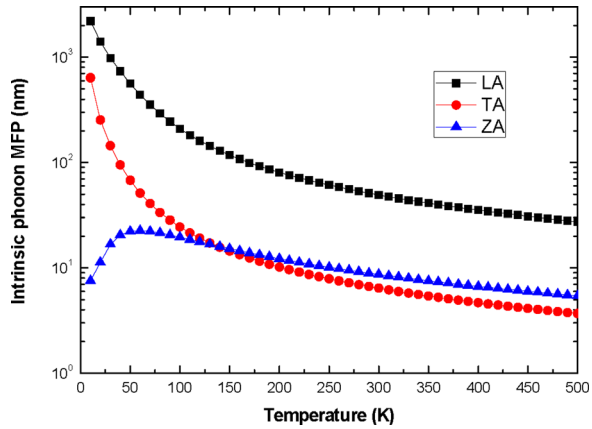

FIG. 2. The intrinsic phonon MFP of LA, TA, and ZA modes as function of temperature.

scattering is much more significant than the phonon-boundary scattering in $MLMoS_2$ even for long wavelength phonons. In SLG, the boundary scattering plays dominant role in scattering of long wavelength phonons, because the Umklapp scattering rate of long wavelength phonons is ultra-low. However, in $MLMoS_2$, because of the huge Grüneisen parameters near Γ point, the Umklapp scattering rate of long wavelength phonons is higher than the boundary scattering rate. Therefore, the phonon MFP in $MLMoS_2$ is mainly limited by the Umklapp phonon-phonon scattering even for long wavelength phonons. The short phonon MFP leads to the length, width, and edge roughness insensitive thermal conductivity observed in $MLMoS_2$ flakes. According to Eq. (10), the intrinsic averaged phonon MFP for all acoustic phonons is given as

$$\bar{\Lambda} = \frac{\sum_\lambda \int_0^{q_{\max}} \Lambda_\lambda(q) \cdot \frac{S}{(2\pi)^2} \cdot \frac{1}{e^{\hbar\omega_\lambda(q)/kT}-1} \cdot 2\pi q \cdot dq}{\sum_\lambda \int_0^{q_{\max}} \frac{S}{(2\pi)^2} \cdot \frac{1}{e^{\hbar\omega_\lambda(q)/kT}-1} \cdot 2\pi q \cdot dq}. \quad (11)$$

It is only 14.6 nm in $MLMoS_2$ at room temperature, which is much shorter than the intrinsic phonon MFP in graphene (700–800 nm).[31,32]

The relative contribution of spectral phonons to the thermal conductivity is an intriguing question in phonon

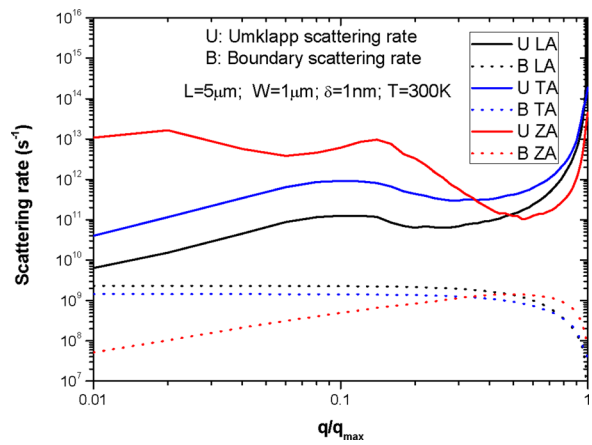

FIG. 3. The phonon-phonon Umklapp scattering rate and phonon-boundary scattering rate as function of wave vector of phonons.

transport of monolayer 2D sheets. Due to the small phonon group velocity, it was suggested that ZA phonons have a much lower contribution than LA and TA phonons to the thermal conductivity of SLG.[26] For an ideal flat free-standing graphene sheet, a selection rule for three-phonon scattering was expected. This selection rule strongly restricts the phase space for umklapp scattering of ZA phonons, which may leads to remarkable increases in ZA modes contributions to the total thermal conductivity of graphene.[33,34] However, in practical 2D devices, the geometry deformation[35–37] and substrate[38,39] will break this selection rule due to loss of reflection symmetry, and thermal conductivity of ZA phonons will be suppressed significantly in geometrically deformed or in the supported monolayer 2D samples. Therefore, this selection rule is not adopted in our calculation of thermal conductivity for $MLMoS_2$ and SLG.

As shown in Fig. 1, the contribution of ZA phonons in $MLMoS_2$ to thermal conductivity is about 33% at room temperature, and the contribution of TA phonons in $MLMoS_2$ is very low (about 7.5%), in contrast to the major contribution of TA phonons in SLG. The distinctions result from the different phonon dispersions and Grüneisen parameters between $MLMoS_2$ and SLG. For SLG, the linear dispersion for in-plane acoustic phonons and the quadratic dispersion for out-of-plane acoustic phonons are almost applicable in the whole first Brillouin zone.[26] For $MLMoS_2$, by first-principle calculation, it was shown that the group velocity of LA and TA phonons markedly decreases with the wave vector, and group velocity of ZA phonons first increases then decreases with the magnitude of wave vector.[4] For SLG, the Grüneisen parameters of LA (around 2.0) and TA (around 0.7) branches have weak dependence on the wave vector, the Grüneisen parameter of ZA branch (between −53 and −1.46) is negative and increases with the wave vector.[40] For $MLMoS_2$, the Grüneisen parameters of all acoustic branches have strong dependence on the wave vector. Near the center of the first Brillouin zone, the Grüneisen parameters are very large (25.3 for LA, 58.6 for TA, and 159.7 for ZA), and they decrease with the increasing magnitude of wave vector.[4] The Grüneisen parameter provides information on the strength of the lattice anharmonicity and the degree of the phonon scattering. The strong anharmonicity in bonding can result in low lattice thermal conductivity in crystals according to Eqs. (3) and (1). In order to analyze the contribution of spectral phonons to heat conduction, we introduce the accumulative thermal conductivity, which is given as

$$\kappa_\lambda(q) = \frac{S}{(2\pi)^2}\int_0^q\int_0^{2\pi}\frac{k_B}{S\delta}\frac{\left[\hbar\omega_\lambda(q)/k_BT\right]^2 e^{\hbar\omega_\lambda(q)/k_BT}}{\left[e^{\hbar\omega_\lambda(q)/k_BT}-1\right]^2} \times v_\lambda^2(q)\cos^2\theta\tau_\lambda(q,\theta)qd\theta dq. \quad (12)$$

The accumulative thermal conductivity of LA, TA, and ZA phonons of $MLMoS_2$ are demonstrated in Fig. 4(a). For ZA phonons with small wave vector, the lower group velocity and the larger Grüneisen parameter than LA and TA phonons result in lower contribution to thermal conductivity. However, beyond 0.35 q_{max}, the group velocity of ZA phonons is higher than that of TA, and beyond 0.5 q_{max}, the group velocity of ZA phonons is higher than both of LA and TA. Moreover, the Grüneisen parameter of ZA is almost equal to that of TA.[4] Therefore, as shown in Fig. 4(a), beyond 0.45 q_{max}, the contribution of ZA phonons to thermal conductivity is over TA phonons, and it increases with an increase in wave vector. This leads to the unusual high contribution from ZA modes to thermal conductivity in $MLMoS_2$.

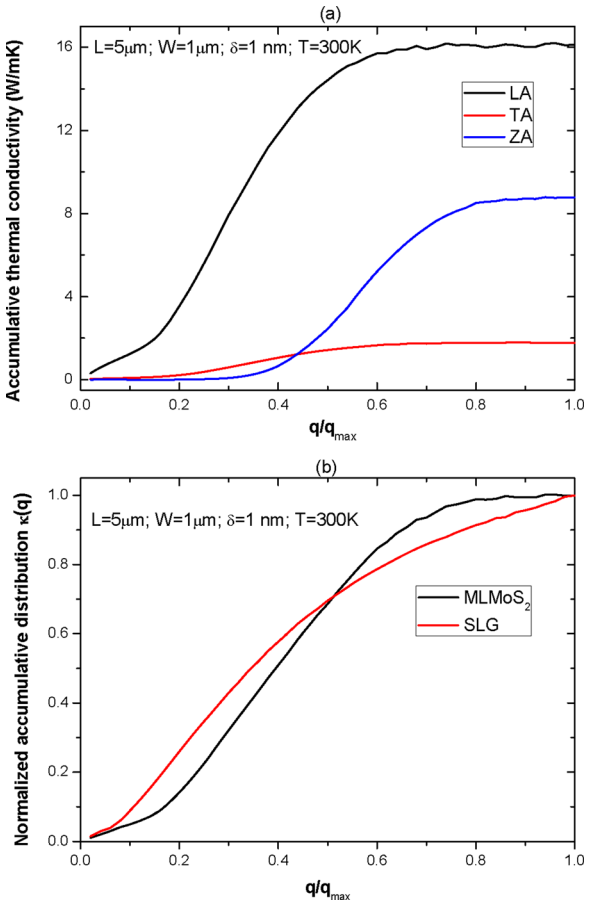

FIG. 4. (a) The accumulative thermal conductivity of spectral phonons as function of wave vector in $MLMoS_2$. (b) The normalized accumulative thermal conductivity of $MLMoS_2$ and SLG as function of wave vector.

Furthermore, we present the normalized accumulative thermal conductivity, which is given as

$$\kappa(q) = \frac{\kappa_{LA}(q)+\kappa_{TA}(q)+\kappa_{ZA}(q)}{\kappa_{LA}+\kappa_{TA}+\kappa_{ZA}}, \quad (13)$$

and compare the normalized accumulative thermal conductivity of $MLMoS_2$ with that of SLG, which is shown in Fig. 4(b). For phonons with wave vector near the center and near the edge of first Brillouin zone, the relative contribution to thermal conductivity of phonons in $MLMoS_2$ is lower than that in SLG, because of the larger Grüneisen parameters near the center of first Brillouin zone, and the lower group velocity near the edge of first Brillouin zone. The underlying reason for the difference in phonon dispersions and Grüneisen parameters between $MLMoS_2$ and SLG may be due to the sandwiched structure of $MLMoS_2$ and the much weaker Mo–S bonds with respect to the strong C–C bonds.

Fig. 5(a) presents the thermal conductivity of $MLMoS_2$ flake as the function of temperature. The roughly $\kappa \propto 1/T$

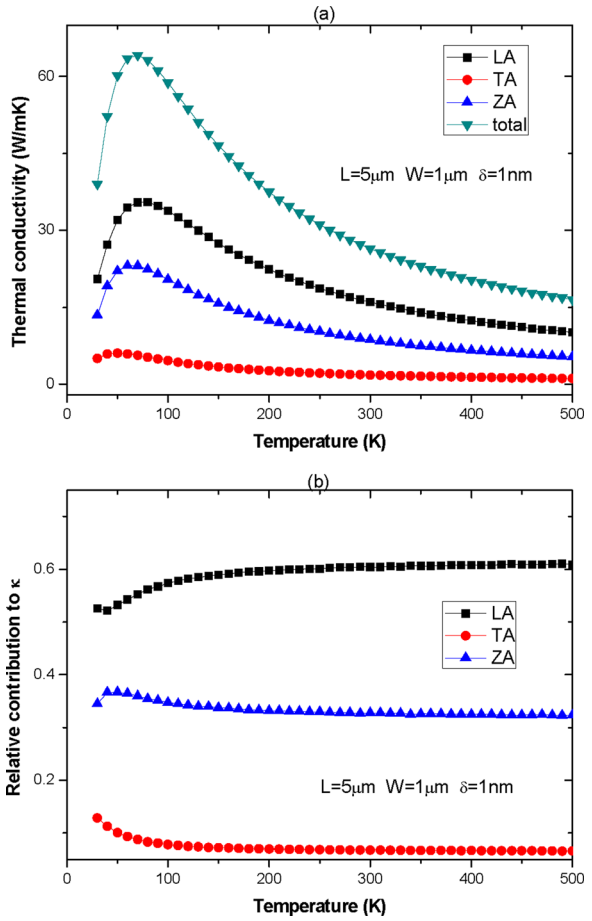

FIG. 5. (a) The thermal conductivity of $MLMoS_2$ flake as a function of temperature. (b) The relative contribution of spectral phonons to thermal conductivity as a function of temperature.

behavior over 70 K results from the dominant phonon-phonon umklapp scattering. Fig. 5(b) gives the temperature-dependent relative contribution of individual phonon branches to the thermal conductivity of $MLMoS_2$. At any temperature, the LA mode has the largest contribution to the thermal conductivity of $MLMoS_2$, and the contribution from ZA modes is considerable.

In summary, we investigate the size and edge roughness dependence on thermal conductivity of $MLMoS_2$ by phonon BTE combined with relaxation time approximation. The relative contribution of spectral phonons to thermal conductivity is explored, and these characteristics of $MLMoS_2$ are compared with that in SLG. The thermal conductivity of $MLMoS_2$, 26.2 W/mK at room temperature, is remarkably lower than that of graphene (~5000 W/mK), which mainly results from the lower group velocities of acoustic phonons, and the larger Grüneisen parameters, especially for low-frequency in-plane phonons. Because of the ultra-short intrinsic phonon MFP (14.6 nm) at room temperature, the thermal conductivity of $MLMoS_2$ flake is size and roughness insensitive. The LA phonons have the major contribution to thermal conductivity of $MLMoS_2$, and the ZA phonons in $MLMoS_2$ have high relative contribution. These distinctions result from the different phonon dispersions and Grüneisen parameters between $MLMoS_2$ and SLG. Our findings are helpful for understanding and engineering the thermal conductivity of $MLMoS_2$ sheet and nanoribbons.

This work was financially supported by National Natural Science Foundation of China (NSFC) (Grant Nos. 11275163, 11274011, 11204262, and 11304264), the Ministry of Education of China (Grant No. 20110001120133), and Scientific Research Fund of Education Department of Hunan Province (No. 13B117).

[1]X. J. Liu, G. Zhang, Q. X. Pei, and Y.-W. Zhang, Appl. Phys. Lett. **103**, 133113 (2013).
[2]W. Li, J. Carrete, and N. Mingo, Appl. Phys. Lett. **103**, 253103 (2013).
[3]J. W. Jiang, H. S. Park, and T. Rabczuk, J. Appl. Phys. **114**, 064307 (2013).
[4]Y. Q. Cai, J. H. Lan, G. Zhang, and Y.-W. Zhang, Phys. Rev. B **89**, 035438 (2014).
[5]J. W. Jiang, X. Zhuang, and T. Rabczuk, Sci. Rep. **3**, 2209 (2013).
[6]S. Sahoo, A. P. S. Gaur, M. Ahmadi, M. J.-F. Guinel, and R. S. Katiyar, J. Phys. Chem. C **117**, 9042 (2013).
[7]R. Yan, J. R. Simpson, S. Bertolazzi, J. Brivio, M. Watson, X. Wu, A. Kis, T. Luo, A. R. Hight Walker, and H. G. Xing, ACS Nano **8**, 986 (2014).
[8]M. Chhowalla, H. S. Shin, G. Eda, L.-J. Li, K. P. Loh, and H. Zhang, Nat. Chem. **5**, 263 (2013).
[9]Y. Cai, G. Zhang, and Y.-W. Zhang, J. Am. Chem. Soc. **136**, 6269 (2014).
[10]M. Buscema, M. Barkelid, V. Zwiller, H. S. J. van der Zant, G. A. Steele, and A. Castellanos-Gomez, Nano Lett. **13**, 358 (2013).
[11]A. A. Balandin, S. Ghosh, W. Bao, I. Calizo, D. Teweldebrhan, F. Miao, and C. N. Lau, Nano Lett. **8**, 902 (2008).
[12]K. M. F. Shahil and A. A. Balandin, Solid State Commun. **152**, 1331 (2012).
[13]M. M. Sadeghi, M. T. Pettes, and L. Shi, Solid State Commun. **152**, 1321 (2012).
[14]E. Pop, V. Varshney, and A. K. Roy, MRS Bull. **37**, 1273 (2012).
[15]A. Balandin and K. L. Wang, Phys. Rev. B **58**, 1544 (1998).
[16]G. Zhang and Y.-W. Zhang, Phys. Status Solidi RRL **7**, 754 (2013).
[17]G. F. Xie, Y. Guo, X. L. Wei, K. W. Zhang, L. Z. Sun, J. X. Zhong, G. Zhang, and Y.-W. Zhang, Appl. Phys. Lett. **104**, 233901 (2014).
[18]K. Kaasbjert, K. S. Thygesen, and W. Jacobsen, Phys. Rev. B **85**, 115317 (2012).
[19]Y. L. Shen, G. F. Xie, X. L. Wei, K. W. Zhang, M. H. Tang, J. X. Zhong, G. Zhang, and Y.-W. Zhang, J. Appl. Phys. **115**, 063507 (2014).
[20]G. F. Xie, Y. L. Shen, X. L. Wei, L. W. Yang, H. P. Xiao, J. X. Zhong, and G. Zhang, Sci. Rep. **4**, 5085 (2014).
[21]D. T. Morelli, J. P. Heremans, and G. A. Slack, Phys. Rev. B **66**, 195304 (2002).
[22]P. G. Klemens, J. Wide Bandgap Mater. **7**, 332 (2000).
[23]G. F. Xie, Y. Guo, B. H. Li, L. W. Yang, K. W. Zhang, M. H. Tang, and G. Zhang, Phys. Chem. Chem. Phys. **15**, 14647 (2013).
[24]Z. Aksamija and I. Knezevic, Appl. Phys. Lett. **98**, 141919 (2011).
[25]J. M. Ziman, *Electrons and Phonons: The Theory of Transport Phenomena in Solids* (Clarendon, Oxford, 1962).
[26]D. L. Nika, E. P. Pokatilov, A. S. Askerov, and A. A. Balandin, Phys. Rev. B **79**, 155413 (2009).
[27]W. J. Evans, L. Hu, and P. Keblinsky, Appl. Phys. Lett. **96**, 203112 (2010).
[28]E. Munoz, J. Lu, and B. I. Yakobson, Nano Lett. **10**, 1652 (2010).
[29]D. L. Nika, A. S. Askerov, and A. A. Balandin, Nano Lett. **12**, 3238 (2012).
[30]X. Xu, L. F. C. Pereira, Y. Wang, J. Wu, K. Zhang, X. Zhao, S. Bae, C. T. Bui, R. Xie, J. T. L. Thong *et al.*, Nat. Commun. **5**, 3689 (2014).
[31]S. Ghosh, I. Calizo, D. Teweldebrhan, E. P. Pokatilov, D. L. Nika, A. A. Balandin, W. Bao, F. Miao, and C. N. Lau, Appl. Phys. Lett. **92**, 151911 (2008).
[32]S. Ghosh, W. Bao, D. L. Nika, S. Subrina, E. P. Pokatilov, C. N. Lau, and A. A. Balandin, Nat. Mater. **9**, 555 (2010).
[33]J. H. Seol, I. Jo, A. L. Moore, L. Lindsay, Z. H. Aitken, M. T. Pettes, X. Li, Z. Yao, R. Huang, D. Broido, N. Mingo, R. S. Ruoff, and L. Shi, Science **328**, 213 (2010).
[34]L. Lindsay, D. A. Broido, and N. Mingo, Phys. Rev. B **82**, 115427 (2010).
[35]V. B. Shenoy, C. D. Reddy, A. Rama, and Y. W. Zhang, Phys. Rev. Lett. **101**, 245501 (2008).
[36]V. B. Shenoy, C. D. Reddy, and Y. W. Zhang, ACS Nano **4**, 4840 (2010).
[37]C. Yu and G. Zhang, J. Appl. Phys. **113**, 044306 (2013).
[38]J. Chen, G. Zhang, and B. Li, Nanoscale **5**, 532 (2013).
[39]C. Yu and G. Zhang, J. Appl. Phys. **113**, 214304 (2013).
[40]B. D. Kong, S. Paul, M. B. Nardelli, and K. W. Kim, Phys. Rev. B **80**, 033406 (2009).